



Original contribution

Longitudinal stability of resting-state networks in normal aging, mild cognitive impairment, and Alzheimer's disease



Hidemasa Takao^{*}, Shiori Amemiya, Osamu Abe, for the Alzheimer's Disease Neuroimaging Initiative¹

Department of Radiology, Graduate School of Medicine, University of Tokyo, 7-3-1 Hongo, Bunkyo-ku, Tokyo 113-8655, Japan

ARTICLE INFO

Keywords:

Default mode network
fMRI
Functional connectivity
Intraclass correlation coefficient
Reproducibility
Test-retest reliability

ABSTRACT

Test-retest reliability is essential for using resting-state functional magnetic resonance imaging (rs-fMRI) as a potential biomarker for Alzheimer's disease (AD), especially when monitoring longitudinal changes and treatment effects. In addition, test-retest variability itself might represent a feature of AD. Using 3.0 T rs-fMRI data from the Alzheimer's Disease Neuroimaging Initiative (ADNI) database, we examined the long-term (1-year) test-retest reliability of resting-state networks (RSNs) in 31 healthy elderly subjects, 63 patients with mild cognitive impairment (MCI), and 17 patients with AD by applying temporal concatenation group independent component analysis and dual regression. The intraclass correlation coefficient estimates of RSN amplitudes ranged from 0.44 to 0.77 in healthy elderly subjects, from 0.31 to 0.62 in patients with MCI, and from -0.06 to 0.44 in patients with AD. The overall test-retest reliability of RSNs was lower in patients with MCI than in healthy elderly subjects, and was lower in patients with AD than in patients with MCI. The differences in the test-retest reliabilities were due to the RSN amplitudes rather than the RSN shapes. Head motion was not significantly different among the three groups of subjects. The results indicate that the test-retest stability of RSNs generally declines with progression to MCI and AD, mainly due to the RSN amplitudes rather than the RSN shapes. The test-retest instability in MCI and AD may reflect progressive neurofunctional alterations related to the pathology of AD.

1. Introduction

Resting-state functional magnetic resonance imaging (rs-fMRI) has been widely used to study the spontaneous fluctuations in brain activity in healthy individuals and in patients with a variety of neurological or psychiatric diseases, since it was first reported that correlated temporal dynamics of blood oxygen level-dependent (BOLD) responses were observed across the sensorimotor cortex, even in resting subjects [1]. Unlike task-based fMRI, rs-fMRI measures brain activity while the subject is resting or in a task-negative state, and the spontaneous fluctuations in the BOLD signal are used to assess whole-brain functional networks and their interrelationships simultaneously without being restricted to one domain by a task. In addition, rs-fMRI is feasible in children and patients with dementia, who are unable to perform the tasks required in task-based fMRI.

Alzheimer's disease (AD) is the most common cause of dementia in older adults. It is an irreversible, progressive neurodegenerative disorder, in which amyloid plaques and neurofibrillary tangles accumulate in the brain, impairing axons, dendrites, and synapses [2]. Despite extensive efforts to develop new treatments for AD, there are currently no drugs that stop or inhibit its progression; currently available drugs temporarily slow the worsening of dementia symptoms and help prevent behavioral problems. To aid drug development and facilitate the treatment of AD, biomarkers are required that can help clinicians track the pathophysiological processes of AD and may temporally precede the development of the known biomarker, amyloid β peptides [3]. rs-fMRI is a candidate imaging biomarker that may bridge this gap because functional connectivity may reveal functional abnormalities before amyloid biomarkers accumulate to a pathologically abnormal level [3,4].

rs-fMRI studies in patients with AD have shown that decreased

* Corresponding author.

E-mail address: takao@tky.umin.ac.jp (H. Takao).

¹ Data used in preparation of this article were obtained from the Alzheimer's Disease Neuroimaging Initiative (ADNI) database (<http://adni.loni.usc.edu>). As such, the investigators within the ADNI contributed to the design and implementation of ADNI and/or provided data but did not participate in analysis or writing of this report. A complete listing of ADNI investigators can be found at: http://adni.loni.usc.edu/wp-content/uploads/how_to_apply/ADNI_Acknowledgement_List.pdf.

Table 1Subject characteristics (mean \pm standard deviation [range]).

	HE	MCI	AD	p^a
<i>n</i>	31	63	17	
Sex				0.27
Female	18	27	10	
Male	13	36	7	
Age (y)	76.0 \pm 7.2 (64.1–94.7)	71.9 \pm 7.0 (56.7–88.7)	74.3 \pm 8.1 (56.0–86.6)	0.04
Education (y)	16.1 \pm 2.3 (12–20)	16.4 \pm 2.5 (11–20)	15.1 \pm 2.5 (12–20)	0.17
MMSE	28.9 \pm 1.2 (26–30)	27.9 \pm 1.7 (24–30)	22.7 \pm 2.3 (19–26)	0.00
Scan interval (y)	1.05 \pm 0.06 (0.92–1.22)	1.03 \pm 0.05 (0.90–1.16)	1.03 \pm 0.07 (0.89–1.19)	0.26

HE, healthy elderly; MCI, mild cognitive impairment; AD, Alzheimer's disease; MMSE, Mini Mental State Examination.

^a χ^2 test (for categorical variables) or Kruskal–Wallis test (for numerical variables).

connectivity affects the default mode network, a large-scale network of interacting brain regions that are active in a resting subject, including the posterior cingulate cortex and precuneus, the medial prefrontal cortex, and the angular gyrus [4–6]. In addition to AD, decreased connectivity in the default mode network is found in mild cognitive impairment (MCI), in unaffected carriers of familial AD, and in subjects with subjective cognitive complaints. In contrast, increased connectivity

in the default mode network is found in healthy subjects with the *APOE4* genotype, a risk factor for AD, possibly as a compensatory response to early subclinical damage [4]. Studies of other networks have yielded mixed and heterogeneous results [6]. The other networks affected by AD progression include the dorsal attention, executive control, salience, and sensorimotor networks [5].

Adequate test–retest reliability is essential for using neuroimaging as

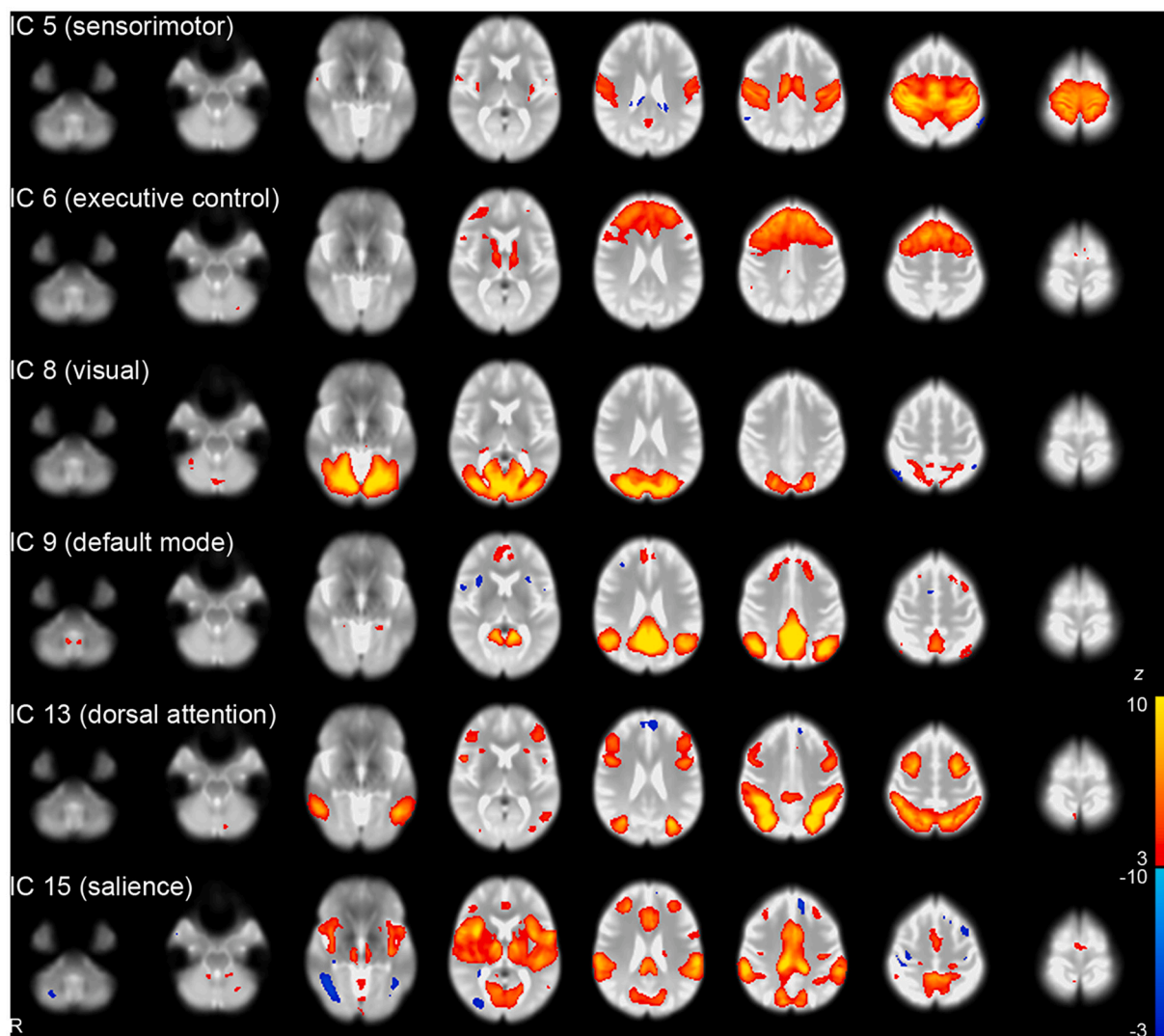


Fig. 1. Resting-state networks obtained by temporal concatenation group independent component analysis, including the sensorimotor, executive control, visual, default mode, dorsal attention, and salience networks. The maps are thresholded at $|z| > 3$. IC, independent component.

Table 2

Intraclass correlation coefficient estimates of the standard deviations of subject-specific time courses generated by dual regression, representing the amplitudes of resting-state networks.

	Overall (95% CI)	HE (95% CI)	MCI (95% CI)	AD (95% CI)
IC 5 (sensorimotor)	0.50 (0.35–0.63)	0.77 (0.57–0.88)	0.42 (0.20–0.61)	0.28 (−0.25–0.67)
IC 6 (executive control)	0.29 (0.12–0.45)	0.47 (0.15–0.70)	0.33 (0.10–0.53)	−0.05 (−0.55–0.45)
IC 8 (visual)	0.45 (0.29–0.58)	0.63 (0.36–0.80)	0.43 (0.21–0.61)	−0.04 (−0.53–0.44)
IC 9 (default mode)	0.53 (0.38–0.65)	0.44 (0.11–0.68)	0.62 (0.44–0.75)	0.27 (−0.24–0.66)
IC 13 (dorsal attention)	0.36 (0.19–0.51)	0.64 (0.37–0.81)	0.31 (0.07–0.51)	−0.06 (−0.53–0.43)
IC 15 (salience)	0.50 (0.33–0.63)	0.65 (0.39–0.81)	0.44 (0.21–0.63)	0.44 (−0.00–0.75)

IC, independent component; CI, confidence interval; HE, healthy elderly; MCI, mild cognitive impairment; AD, Alzheimer's disease.

Table 3

Within-subject coefficient of variation estimates of the standard deviations of subject-specific time courses generated by dual regression, representing the amplitudes of resting-state networks.

	Overall (95% CI)	HE (95% CI)	MCI (95% CI)	AD (95% CI)
IC 5 (sensorimotor)	25.3% (21.7–28.4%)	18.0% (13.7–21.4%)	27.1% (22.2–31.2%)	29.4% (16.9–38.0%)
IC 6 (executive control)	28.5% (23.6–32.6%)	24.3% (12.4–32.0%)	28.9% (23.1–33.7%)	33.7% (13.8–45.6%)
IC 8 (visual)	26.1% (22.4–29.4%)	23.6% (17.6–28.3%)	25.7% (20.6–29.9%)	31.7% (17.9–41.1%)
IC 9 (default mode)	16.7% (13.7–19.2%)	15.2% (11.0–18.4%)	16.7% (13.0–19.8%)	19.1% (0.0–27.3%)
IC 13 (dorsal attention)	19.8% (16.5–22.7%)	14.4% (9.6–18.0%)	20.9% (16.4–24.6%)	23.9% (11.9–31.6%)
IC 15 (salience)	17.8% (15.6–19.8%)	15.4% (10.7–19.0%)	19.3% (16.4–21.7%)	16.4% (9.0–21.3%)

IC, independent component; CI, confidence interval; HE, healthy elderly; MCI, mild cognitive impairment; AD, Alzheimer's disease.

Table 4

Means and standard deviations (SDs) of the standard deviations of subject-specific time courses generated by dual regression, representing the amplitudes of resting-state networks.

	Screening			At 1 year		
	HE (SD)	MCI (SD)	AD (SD)	HE (SD)	MCI (SD)	AD (SD)
IC 5 (sensorimotor)	3.70 (1.57)	3.88 (1.62)	3.91 (1.66)	4.10 (1.79)	4.19 (1.52)	3.96 (1.67)
IC 6 (executive control)	4.12 (1.98)	4.10 (1.52)	4.96 (2.69)	4.51 (2.33)	4.75 (2.25)	4.89 (2.30)
IC 8 (visual)	3.58 (1.97)	3.40 (1.34)	3.17 (0.85)	3.69 (1.47)	3.63 (1.35)	3.48 (1.72)
IC 9 (default mode)	3.32 (0.75)	3.51 (1.02)	3.22 (0.69)	3.48 (0.77)	3.49 (1.00)	3.43 (1.23)
IC 13 (dorsal attention)	3.20 (0.79)	3.45 (1.03)	3.23 (0.56)	3.40 (1.21)	3.56 (1.02)	3.46 (1.15)
IC 15 (salience)	3.07 (0.90)	2.97 (0.76)	2.96 (0.62)	3.18 (0.83)	3.32 (0.83)	3.29 (0.96)

IC, independent component; HE, healthy elderly; MCI, mild cognitive impairment; AD, Alzheimer's disease.

Table 5

Within-subject standard deviations of the standard deviations of subject-specific time courses generated by dual regression, representing the amplitudes of resting-state networks.

	HE	MCI	AD
IC 5 (sensorimotor)	0.82	1.20	1.38
IC 6 (executive control)	1.57	1.62	2.48
IC 8 (visual)	1.05	1.02	1.36
IC 9 (default mode)	0.57	0.62	0.84
IC 13 (dorsal attention)	0.62	0.85	0.91
IC 15 (salience)	0.51	0.62	0.62

IC, independent component; HE, healthy elderly; MCI, mild cognitive impairment; AD, Alzheimer's disease.

a potential biomarker for AD, especially when monitoring the longitudinal changes of AD and the effects of treatments. Previous studies have evaluated the reliabilities of volumetric T1-weighted imaging [7–15], diffusion imaging [16–20], and rs-fMRI [21–25]; however, few studies have evaluated the test-retest reliability of rs-fMRI in healthy elderly subjects [26–30], patients with MCI [31,32], and patients with AD [33].

Using rs-fMRI data obtained from the Alzheimer's Disease Neuro-imaging Initiative (ADNI) database, we examined the long-term (1-year) test-retest reliability of resting-state networks (RSNs) in healthy elderly subjects, patients with MCI, and patients with AD using temporal concatenation group independent component analysis (ICA) and dual regression [34].

2. Materials and Methods

2.1. Subjects

The data used in this study were obtained from the ADNI database (available at <http://adni.loni.usc.edu>). The ADNI was launched in 2003 as a public-private partnership, led by the Principal Investigator Michael W. Weiner, MD. The primary goal of ADNI was to test whether serial MRI, positron emission tomography (PET), other biological markers, and clinical and neuropsychological assessment can be combined to measure the progression of MCI and early AD. The ADNI was approved by the institutional review boards of all participating sites. Written informed consent was obtained from all participants.

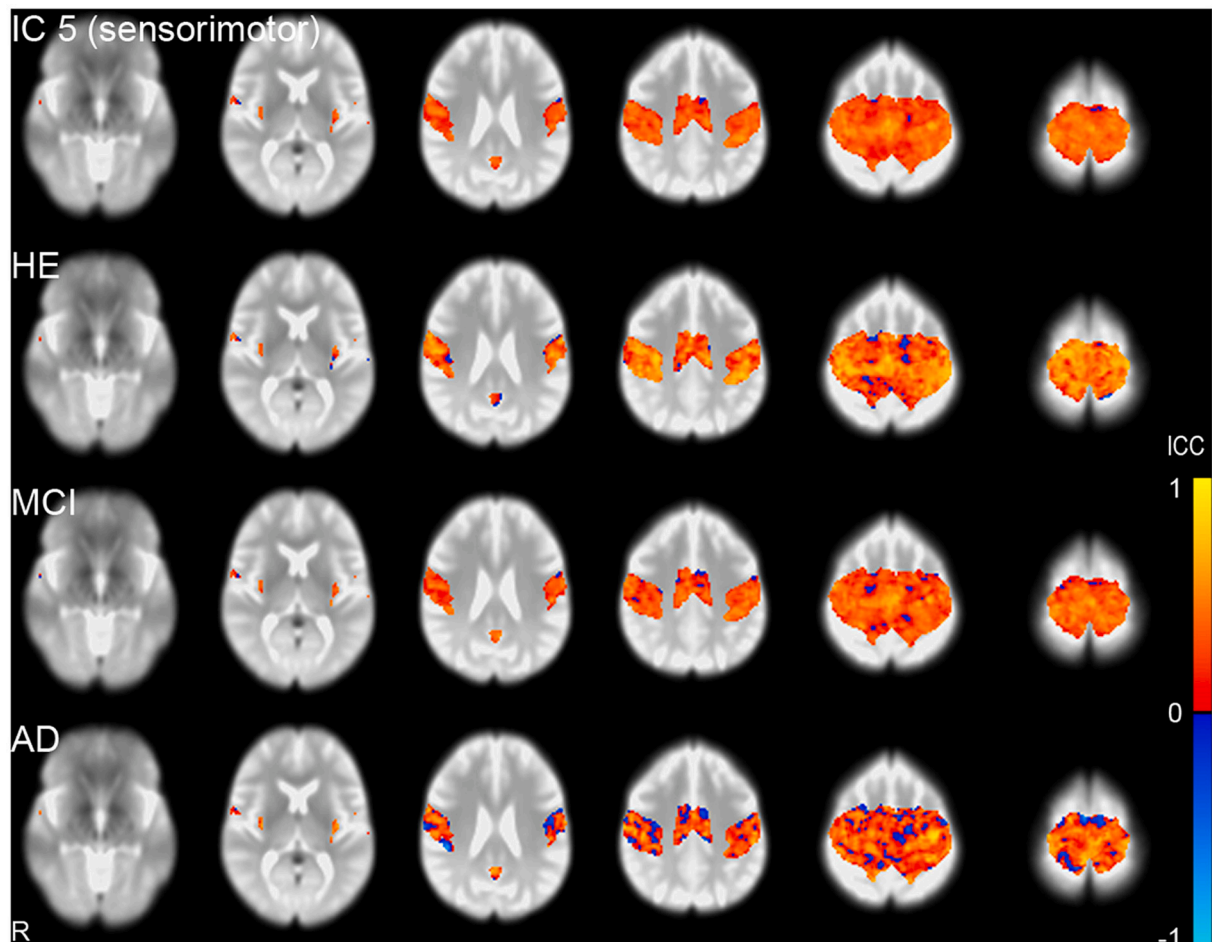


Fig. 2. Voxel-wise intraclass correlation coefficient (ICC) maps of subject-specific spatial maps with variance normalization of the subject-specific time courses during dual regression, representing resting-state network (RSN) shapes and amplitudes. The RSN masks are applied at a threshold of $z > 3$. IC, independent component; HE, healthy elderly; MCI, mild cognitive impairment; AD, Alzheimer's disease.

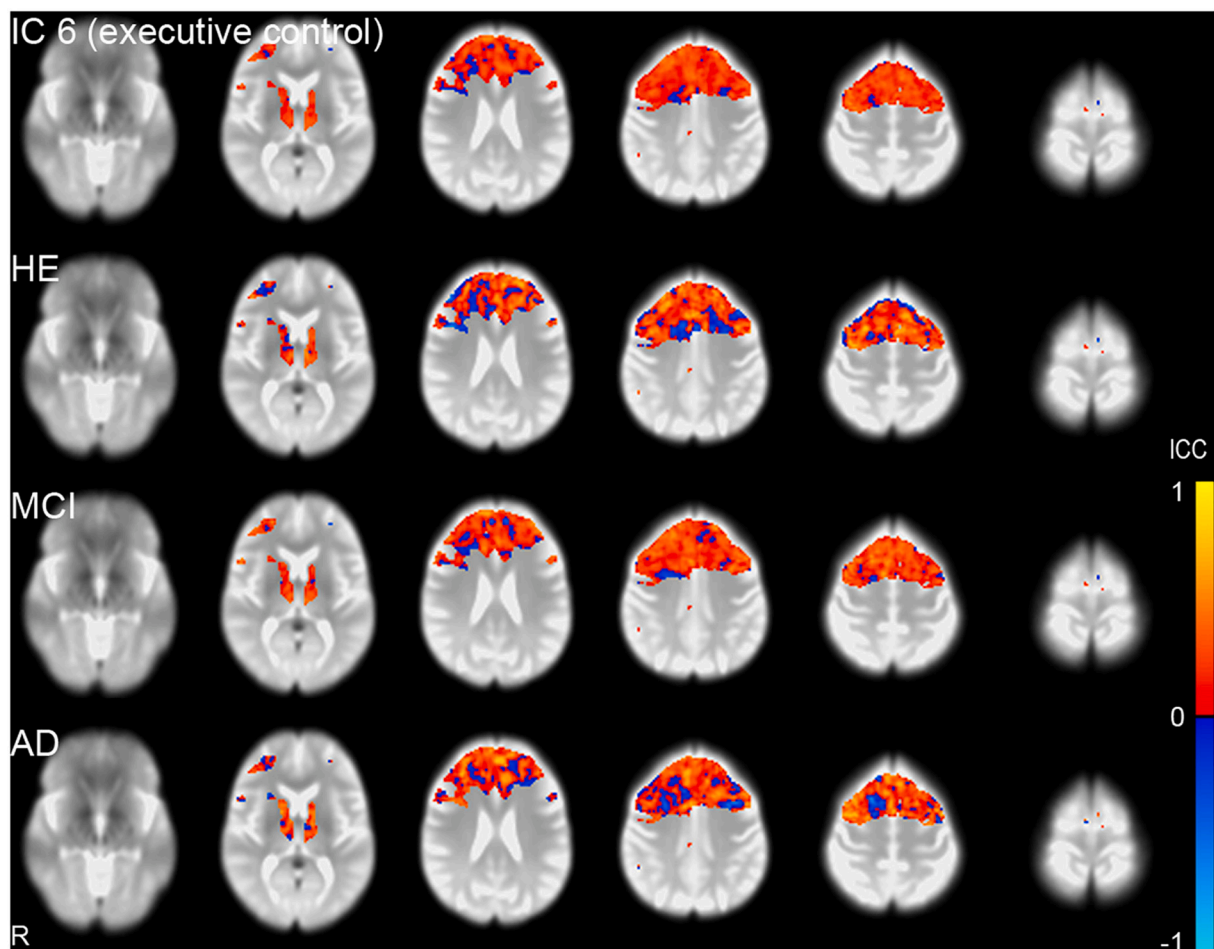


Fig. 2. (continued).

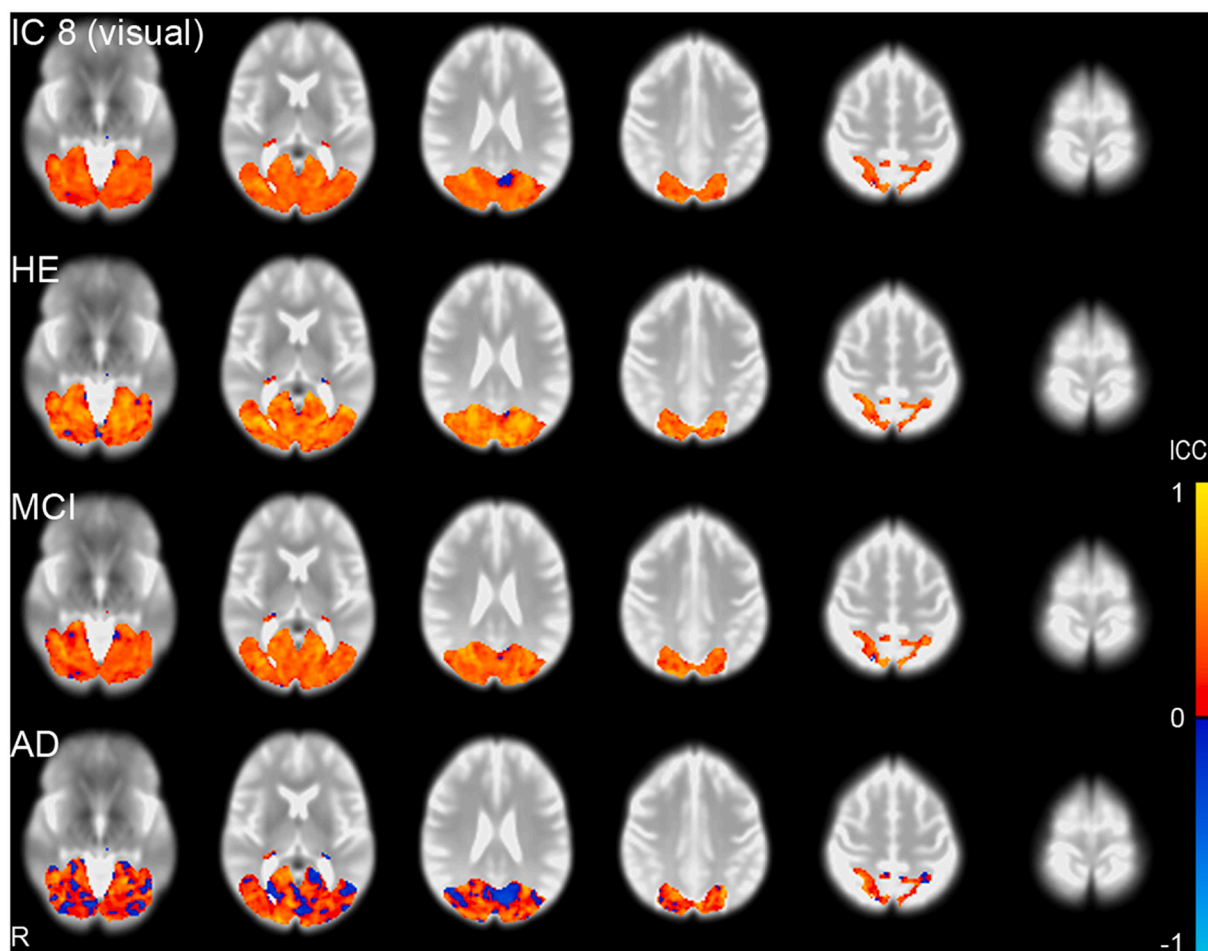


Fig. 2. (continued).

The present study used data selected from the ADNI 2 database comprising subjects with rs-fMRI data from screening and 1 year later. Data with different scan parameters or poor image quality (by visual inspection with reference to quality scores by ADNI quality control at Mayo Clinic) were excluded. AD was diagnosed according to the National Institute of Neurological and Communicative Disorders and Stroke-Alzheimer's Disease and Related Disorders Association (NINCDS-ADRDA) criteria, and MCI was diagnosed according to the Mayo Clinic criteria. For details, please refer to the ADNI 2 protocol. A total of 111 subjects (31 healthy control subjects [18 females and 13 males], 63 patients with MCI [27 females and 36 males], and 17 patients with AD [10 females and 7 males]) were included in the present study (Table 1). The mean age (range) at screening was 73.4 ± 7.4 years (healthy control subjects, 76.0 ± 7.2 years [64.1–94.7 years]; patients with MCI, 71.9 ± 7.0 years [56.7–88.7 years]; patients with AD, 74.3 ± 8.1 years [56.0–86.6 years]). The mean scan interval (range) was 1.04 ± 0.06 years (healthy control subjects, 1.05 ± 0.06 years [0.92–1.22 years]; patients with MCI, 1.03 ± 0.05 years [0.90–1.16 years]; patients with AD, 1.03 ± 0.07 years [0.89–1.19 years]).

2.2. Imaging Data Acquisition

MR data were obtained on 3.0 T Philips scanners at multiple sites using the same ADNI 3.0 T imaging protocol. Various models of scanners were used in the ADNI (for details, please refer to <http://adni.loni.usc.edu>), but each subject underwent scans at screening and follow-up on the same scanner.

The rs-fMRI images were acquired using a single-shot gradient-echo echo-planar sequence in 48 axial slices (repetition time = 3000 ms; echo time = 30 ms; flip angle = 80°; field of view = 212 × 199 mm; slice thickness = 3.31 mm with no gap; acquisition matrix = 64 × 59; image matrix = 64 × 64; reconstructed voxel size = 3.31 × 3.31 × 3.31 mm). A total of 140 volumes were acquired with a scan time of 7 min. The subjects were instructed to keep their eyes open during imaging.

Structural T1-weighted images were acquired using a three-dimensional magnetization-prepared rapid gradient-echo (MP-RAGE) sequence in 170 sagittal slices (repetition time = 6.8 ms; echo time = 3.1 ms; inversion time = 900 ms; flip angle = 9°; field of view = 256 × 240 mm; slice thickness = 1.2 mm with no gap; acquisition matrix = 256 × 240; image matrix = 256 × 256; reconstructed voxel size = 1.0 × 1.0 × 1.2 mm). The MP-RAGE images were corrected for intensity non-uniformity using the non-parametric non-uniform intensity normalization algorithm N3 [35–37].

2.3. Image Processing

The rs-fMRI images were mainly processed using FSL (FMRIB Software Library) 5.0.9 software (<http://www.fmrib.ox.ac.uk/fsl>; developed at the Oxford Centre for Functional MRI of the Brain, Nuffield Department of Clinical Neurosciences, John Radcliffe Hospital, University of Oxford, Oxford, UK) [38] and MATLAB 9.1 (Mathworks, Sherborn, MA).

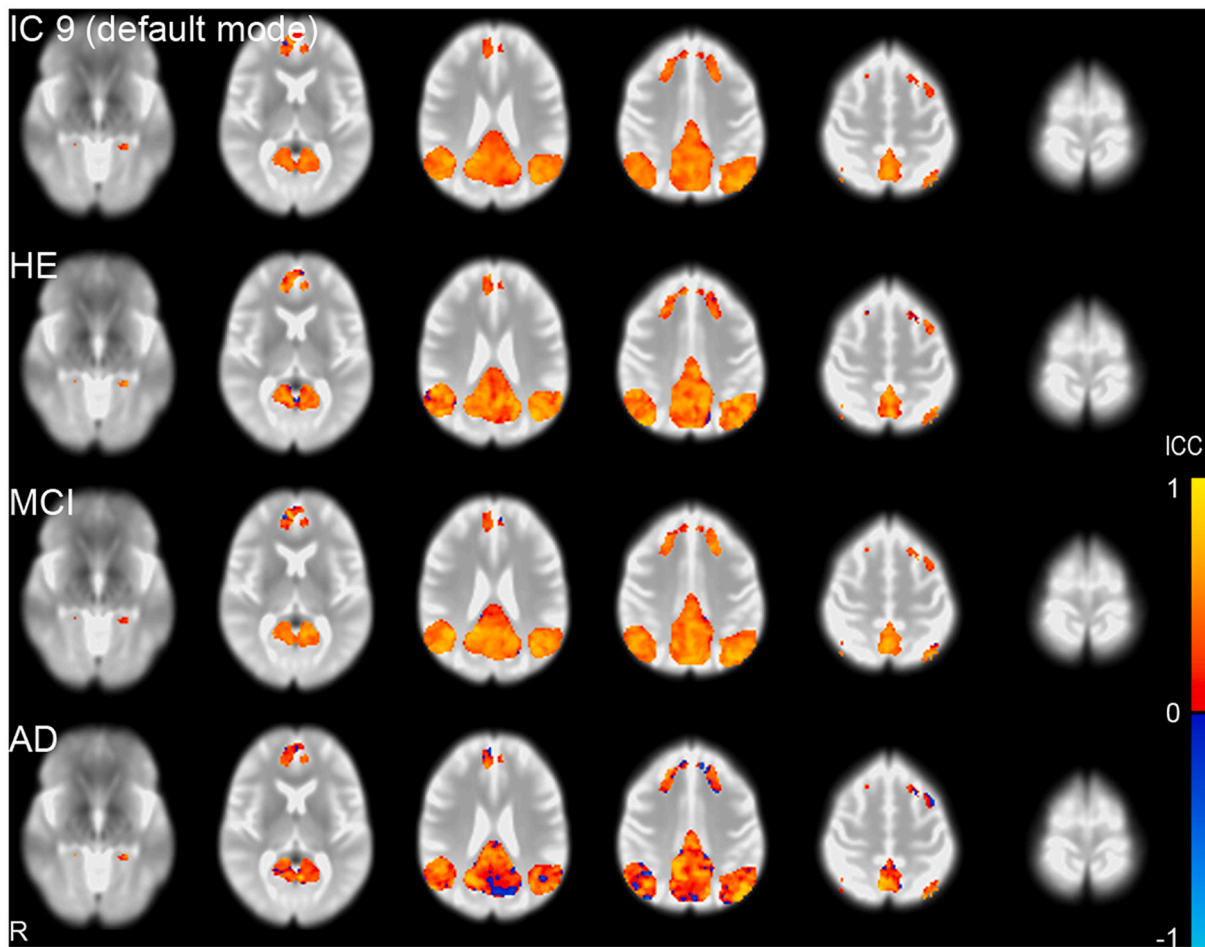


Fig. 2. (continued).

2.3.1. Preprocessing

The images were preprocessed as follows: the first four volumes were discarded due to magnetization instability; motion correction using MCFLIRT [39]; non-brain removal using a brain extraction tool (BET) [40]; spatial smoothing using a Gaussian kernel of full width at half maximum (FWHM) of 5 mm; grand-mean intensity normalization of the entire four-dimensional (4D) dataset by a single multiplicative factor; and high-pass temporal filtering (Gaussian-weighted least-squares straight line fitting, with sigma = 50 s). Briefly, spatial normalization involved the following steps: co-registration to high-resolution structural T1-weighted images by boundary-based registration (BBR) [41] using epi_reg; registration from high-resolution structural to standard space using the FMRIB's linear image registration tool (FLIRT) [39], further improved by the FMRIB's nonlinear registration tool (FNIRT) [38]; creation of a custom echo-planar image template; and registration to the custom echo-planar image template using FNIRT. The final resampled voxel size was $2 \times 2 \times 2$ mm.

2.3.2. ICA

Temporal concatenation group ICA was carried out using probabilistic ICA [42], as implemented in MELODIC (multivariate exploratory linear decomposition into independent components) 3.14. The input data were preprocessed as follows: masking of non-brain voxels; voxel-

wise de-meaning of the data; and normalization of the voxel-wise variance. The preprocessed data were whitened and projected into a 20-dimensional subspace [43] using principal component analysis. The whitened observations were decomposed into sets of vectors describing signal variation across the temporal (time courses) and spatial (maps) domains by optimizing for non-Gaussian spatial source distributions using a fixed-point iteration technique [44]. Estimated component maps were divided by the standard deviation (SD) of the residual noise and thresholded by fitting a mixture model to the intensity histogram [42].

2.3.3. Dual Regression

The spatial maps derived from group ICA were used to generate subject-specific spatial maps with associated time courses by applying dual regression [34]. First, for each subject, the group-level spatial maps were regressed (as spatial regressors in a multiple regression) into the subject's 4D space-time dataset. This resulted in a set of subject-specific time courses, one per group-level spatial map. Next, the time courses were regressed (as temporal regressors in a multiple regression) into the same 4D dataset, resulting in a set of subject-specific spatial maps, one per group-level spatial map. Dual regression was performed with and without variance normalization of the time courses created by spatial regression.

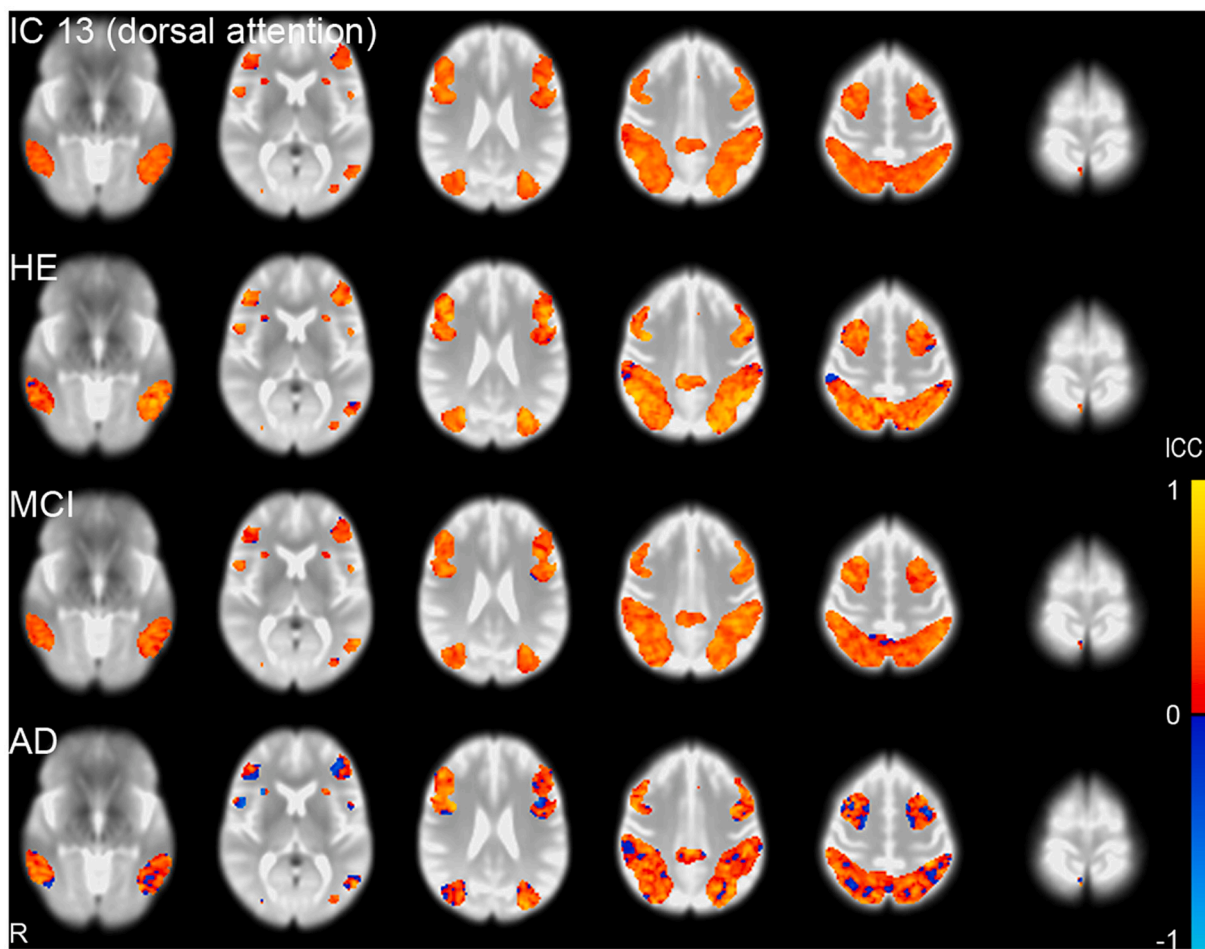


Fig. 2. (continued).

2.3.4. Measurement of Head Motion

The mean absolute and relative displacements calculated by MCFLIRT during motion correction were used to estimate head motion during the scans.

2.4. Statistical Analysis

The SD of subject-specific time courses generated by dual regression represents the RSN amplitude. Intraclass correlation coefficient (ICC) estimates with 95% confidence intervals (CIs) were calculated for the test-retest reliability based on a single-measurement, absolute-agreement, two-way mixed-effects model [45,46] using SPSS Statistics 22 (IBM Corporation, Armonk, NY). Estimates of the within-subject coefficient of variation (CV) with 95% CIs were calculated based on the root mean square method using Excel 2016 (Microsoft Corporation, Redmond, WA), as well as means, SDs, and within-subject SDs.

In addition, the ICC was calculated for each voxel in subject-specific spatial maps (both with and without variance normalization of the subject-specific time courses during dual regression) based on a single-measurement, absolute-agreement, two-way mixed-effects model [45,46] using MATLAB 9.1 as follows:

$$ICC = \frac{MS_R - MS_E}{MS_R + (k-1)MS_E + \frac{k}{n}(MS_C - MS_E)}$$

where

$$MS_R \text{ (mean square for rows)} = \frac{SS_R}{n-1},$$

$$MS_C \text{ (mean square for columns)} = \frac{SS_C}{k-1},$$

$$MS_E \text{ (mean square for error)} = \frac{SS_E}{(n-1)(k-1)},$$

$$SS_T \text{ (total sum of squares)} = \sum x_T^2 - \frac{(\sum x_T)^2}{N},$$

$$SS_R \text{ (sum of squares for rows)} = \sum_i^n \frac{(\sum x_i)^2}{k} - \frac{(\sum x_T)^2}{N},$$

$$SS_C \text{ (sum of squares for columns)} = \sum_j^k \frac{(\sum x_j)^2}{n} - \frac{(\sum x_T)^2}{N},$$

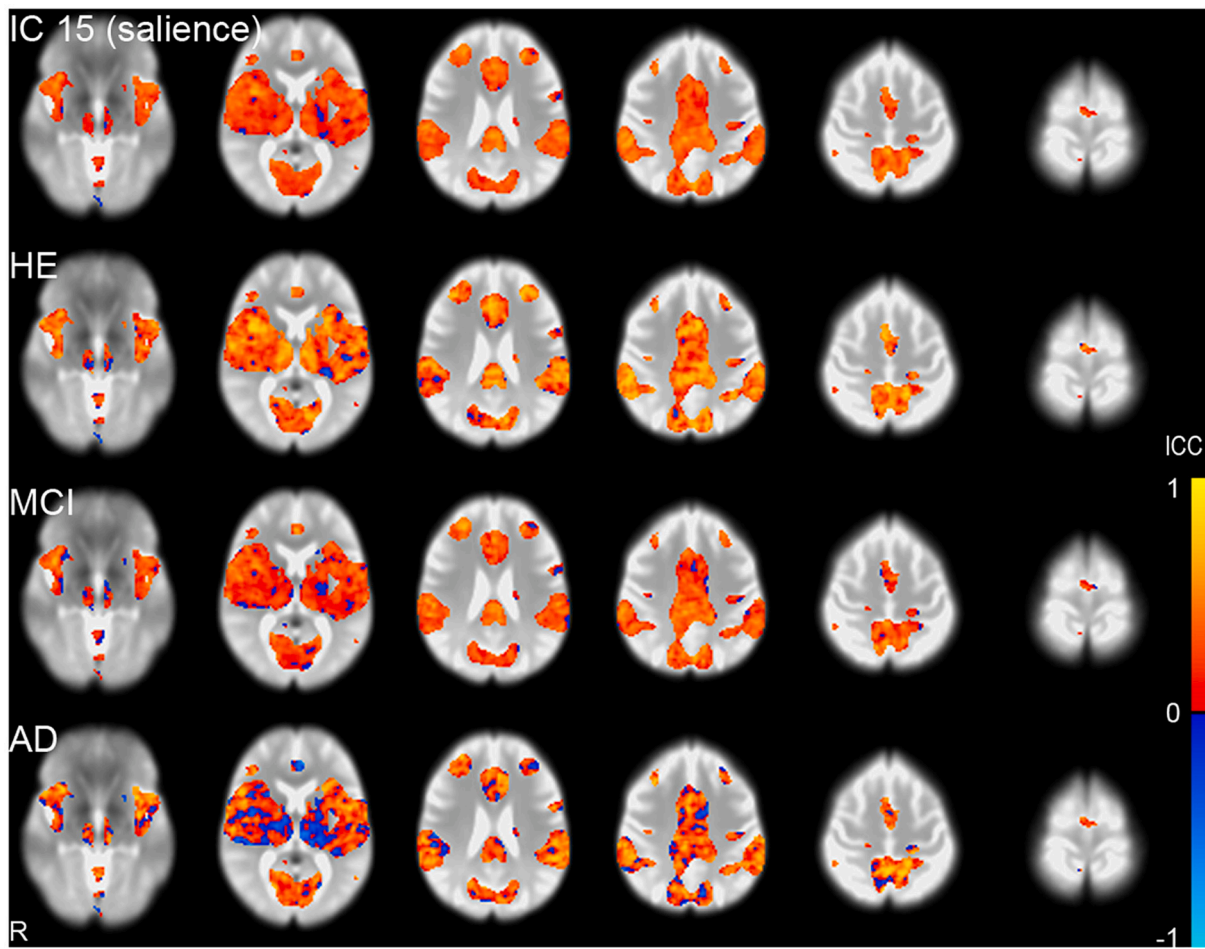


Fig. 2. (continued).

$$SS_E \text{ (sum of squares for error)} = SS_T - SS_R - SS_C,$$

$$\sum x_T = \sum_i^n \sum_j^k x_{ij}, \sum x_T^2 = \sum_i^n \sum_j^k x_{ij}^2,$$

$$N = n \times k, n = \text{number of subjects (rows)}, k = \text{number of measurements (columns) (here 2)}$$

The subject-specific spatial maps with variance normalization of the subject-specific time courses during dual regression represent both RSN shapes and amplitudes, while the subject-specific spatial maps without variance normalization of the subject-specific time courses during dual regression represent only RSN shapes [34].

Histogram analysis was performed for each ICC map with a histogram bin width of 0.02 and a range of -1.0 to 1.0 within a mask for that particular RSN at a threshold of $z > 3$.

Finally, to evaluate the effect of head motion on test-retest reliability, we used 2×3 mixed analysis of variance (ANOVA) to compare the effects of scan (a within-subject factor) and diagnosis (a between-subject factor) on mean absolute and relative displacements (calculated by MCFLIRT) using SPSS Statistics 22.

3. Results

3.1. ICA Maps

Fig. 1 shows six RSNs obtained from the temporal concatenation group ICA, including the sensorimotor, executive control, visual, default mode, dorsal attention, and salience networks.

3.2. Test–Retest Reliability of the Amplitudes of Subject-specific Time Courses

Table 2 shows the ICC estimates with 95% CIs for the SDs of the subject-specific time courses generated by dual regression, representing RSN amplitudes. Overall, the ICCs were lower in patients with MCI than in healthy control subjects (except for IC 9 [default mode network]), and were lower in patients with AD than in patients with MCI. The ICC estimates ranged from 0.44 to 0.77 in healthy control subjects, from 0.31 to 0.62 in patients with MCI, and from -0.06 to 0.44 in patients with AD.

Table 3 shows the within-subject CV estimates with 95% CIs for the SDs of the subject-specific time courses generated by dual regression. The CVs were higher in patients with MCI than in healthy control subjects, and were higher in patients with AD than in patients with MCI.

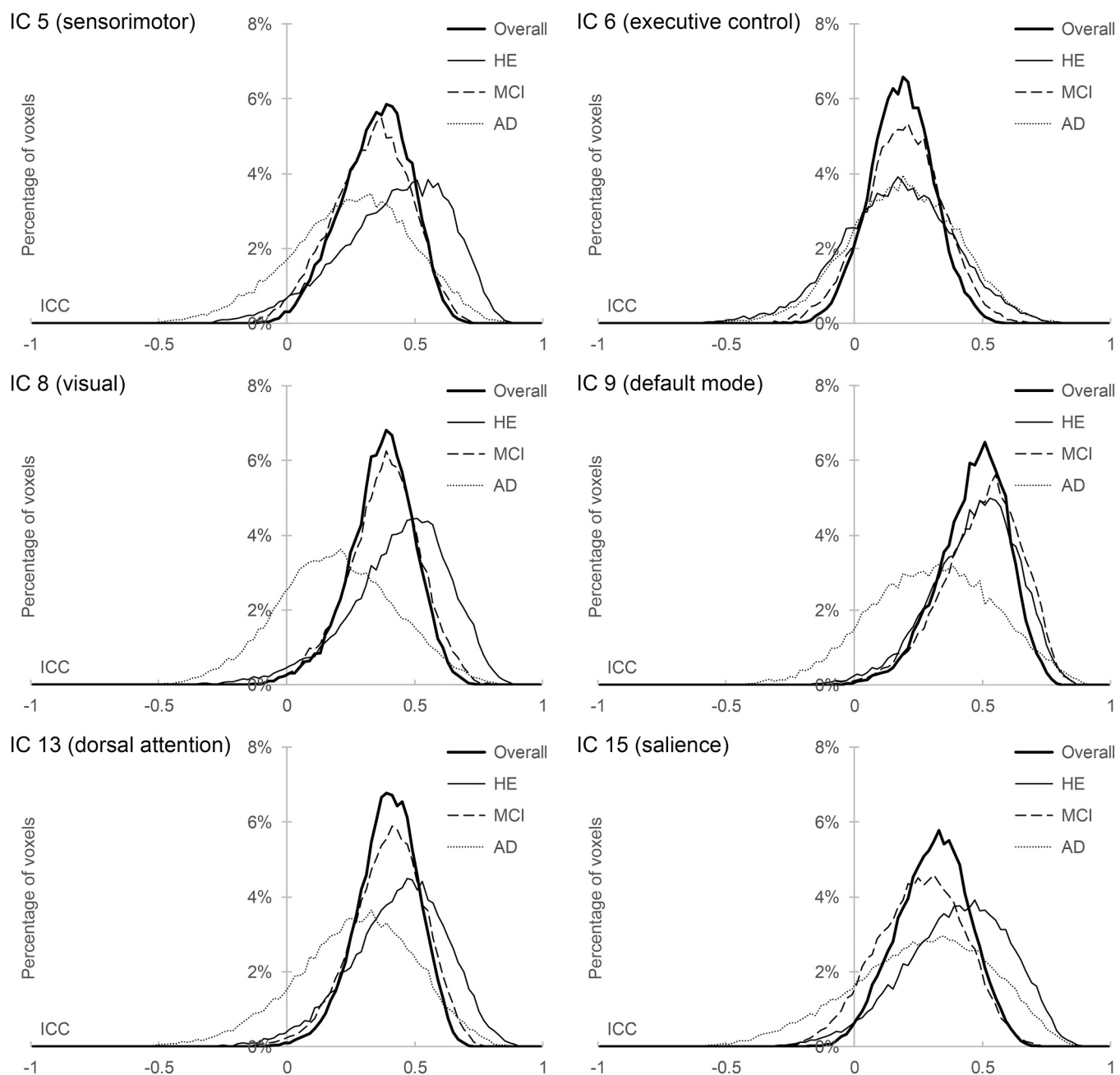


Fig. 3. Histograms (frequency polygons) of voxel-wise intraclass correlation coefficient (ICC) maps of subject-specific spatial maps with variance normalization of the subject-specific time courses during dual regression, representing resting-state network shapes and amplitudes. IC, independent component; HE, healthy elderly; MCI, mild cognitive impairment; AD, Alzheimer's disease.

Table 6

Peaks in the histograms of intraclass correlation coefficient maps of subject-specific spatial maps with variance normalization of the subject-specific time courses during dual regression, representing resting-state network shapes and amplitudes.

	Overall	HE	MCI	AD
IC 5 (sensorimotor)	0.38–0.40	0.54–0.56	0.36–0.38	0.32–0.34
IC 6 (executive control)	0.18–0.20	0.16–0.18	0.20–0.22	0.18–0.20
IC 8 (visual)	0.38–0.40	0.50–0.52	0.38–0.40	0.20–0.22
IC 9 (default mode)	0.50–0.52	0.52–0.54	0.54–0.56	0.32–0.34
IC 13 (dorsal attention)	0.38–0.40	0.46–0.48	0.40–0.42	0.32–0.34
IC 15 (salience)	0.32–0.34	0.46–0.48	0.30–0.32	0.34–0.36

IC, independent component; HE, healthy elderly; MCI, mild cognitive impairment; AD, Alzheimer's disease.

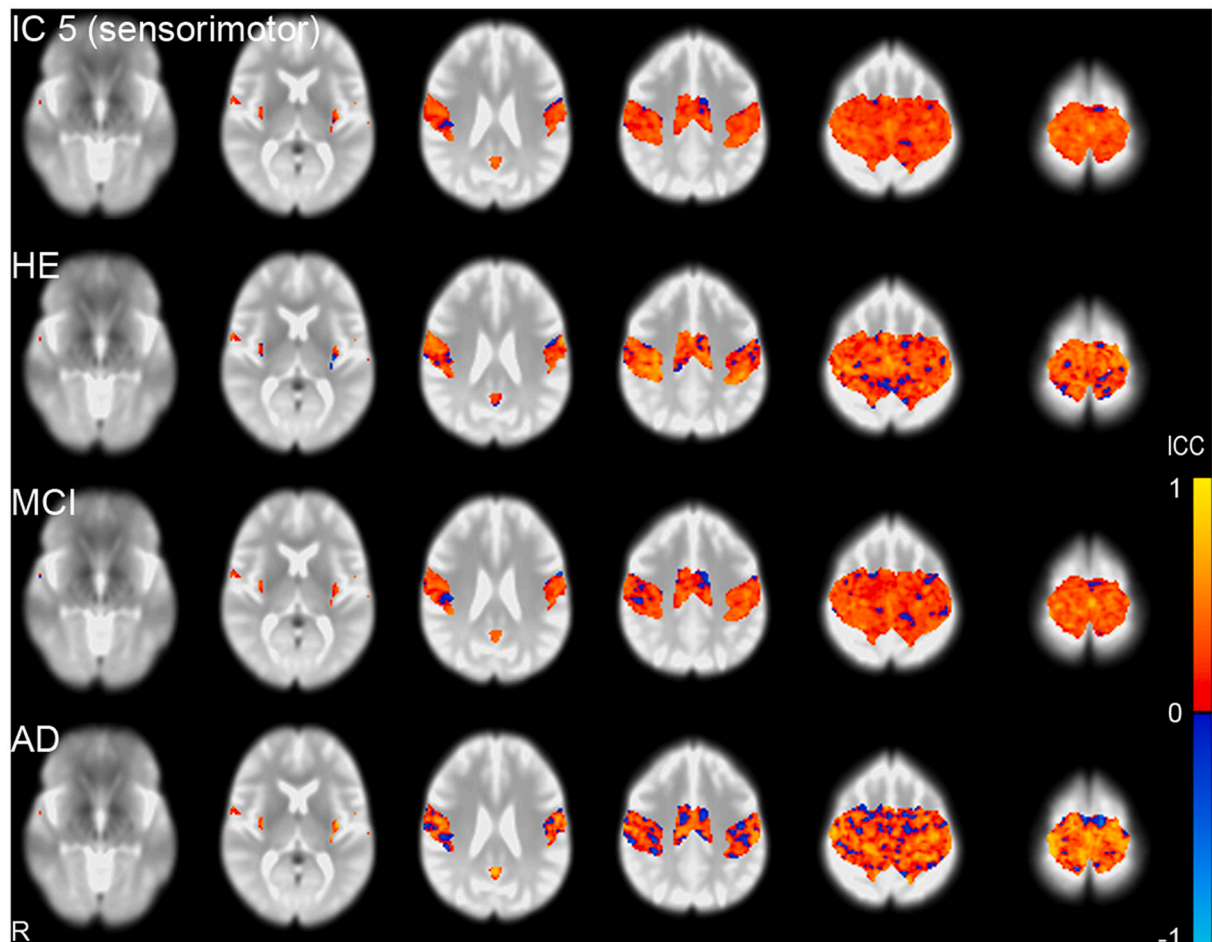


Fig. 4. Voxel-wise intraclass correlation coefficient (ICC) maps of subject-specific spatial maps without variance normalization of the subject-specific time courses during dual regression, representing resting-state network (RSN) shapes. The RSN masks are applied at a threshold of $z > 3$. IC, independent component; HE, healthy elderly; MCI, mild cognitive impairment; AD, Alzheimer's disease.

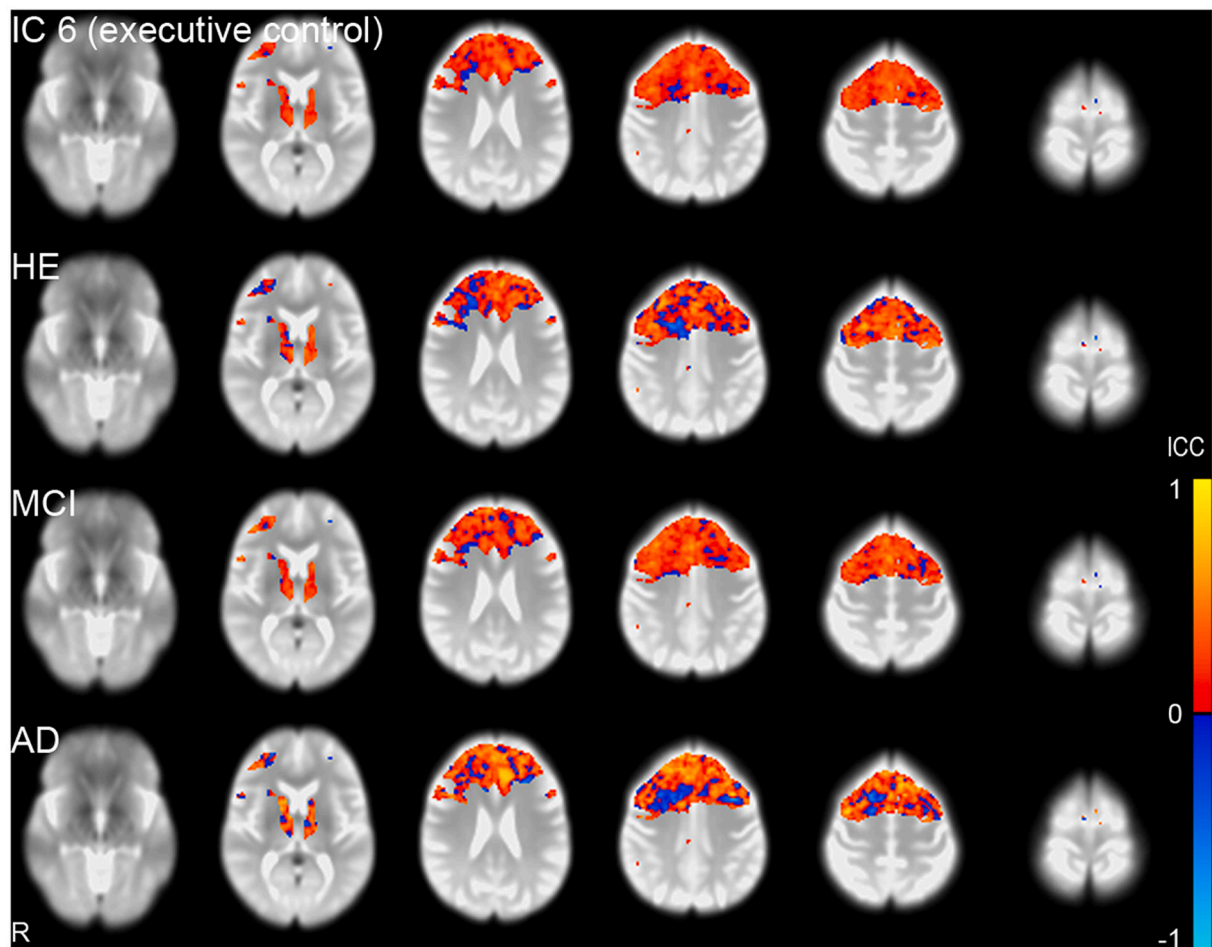


Fig. 4. (continued).

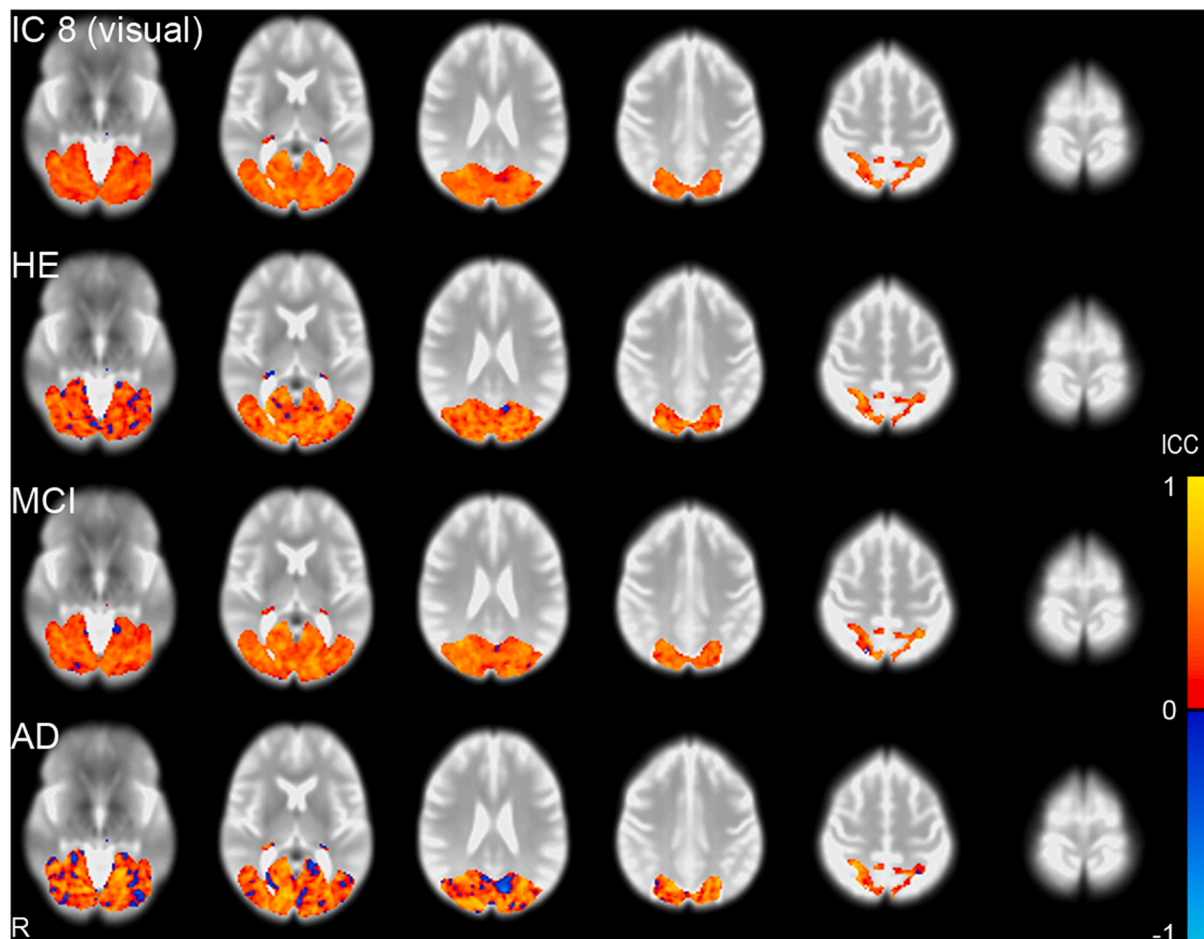


Fig. 4. (continued).

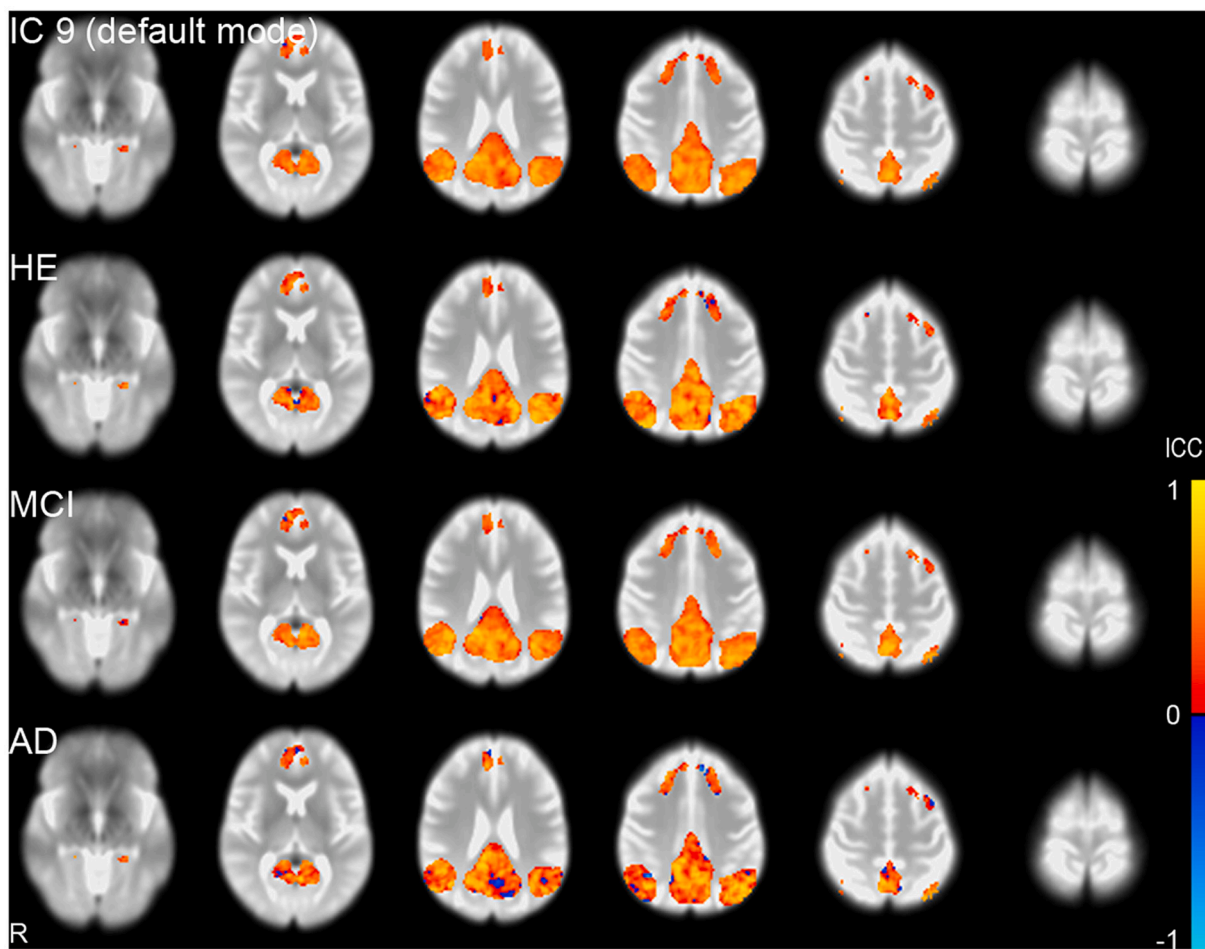


Fig. 4. (continued).

(except for IC 15 [salience network]). The CVs ranged from 14.4% to 24.3% in healthy control subjects, from 16.7% to 28.9% in patients with MCI, and from 16.4% to 33.7% in patients with AD.

Table 4 shows the means and SDs for the SDs of the subject-specific time courses generated by dual regression. Table 5 shows the within-subject SDs for the SDs of the subject-specific time courses generated by dual regression.

3.3. Voxel-wise Test-Retest Reliability of Subject-specific Spatial Maps

Fig. 2 shows the voxel-wise ICC maps of subject-specific spatial maps with variance normalization of the subject-specific time courses during dual regression, representing RSN shapes and amplitudes [34]. Fig. 3 and Table 6 show the results of histogram analysis (frequency polygons and histogram peaks) of the ICC maps. Overall, the histogram peaks were lower in patients with MCI than in healthy control subjects (except for IC 6 [executive control network] and IC 9 [default mode network]), and were lower in patients with AD than in patients with MCI (except for IC15 [salience network]).

Fig. 4 shows the voxel-wise ICC maps of subject-specific spatial maps without variance normalization of the subject-specific time courses during dual regression, representing RSN shapes [34]. Fig. 5 and Table 7 show the results of histogram analysis (frequency polygons and histogram peaks) of the ICC maps. Overall, there were small differences in the histograms among healthy control subjects, patients with MCI, and

patients with AD relative to the ICC maps of subject-specific spatial maps with variance normalization of the subject-specific time courses.

3.4. Head Motion

Fig. 6 shows the mean absolute and relative displacements, which represent head motion during scanning. There were no significant main effects of scan ($F_{(1, 108)} = 0.17, p = 0.68$) or diagnosis ($F_{(2, 108)} = 0.85, p = 0.43$) on the mean absolute displacement. Furthermore, there was no significant interaction of scan \times diagnosis ($F_{(2, 108)} = 0.15, p = 0.86$). At the screening scan, the mean absolute displacements were 0.20 ± 0.10 , 0.18 ± 0.09 , and 0.19 ± 0.08 mm for healthy control subjects, patients with MCI, and patients with AD, respectively. At 1 year, the corresponding values were 0.21 ± 0.22 , 0.18 ± 0.09 , and 0.21 ± 0.10 mm, respectively.

For the mean relative displacement, there was no significant main effect of diagnosis ($F_{(2, 108)} = 0.16, p = 0.85$) but a significant main effect of scan ($F_{(1, 108)} = 4.96, p = 0.03$). There was no significant interaction of scan \times diagnosis ($F_{(2, 108)} = 1.29, p = 0.28$). At the screening scan, the mean relative displacements were 0.14 ± 0.07 , 0.13 ± 0.07 , and 0.13 ± 0.05 mm for healthy control subjects, patients with MCI, and patients with AD, respectively. At 1 year, the corresponding values were 0.14 ± 0.07 , 0.15 ± 0.08 , and 0.16 ± 0.08 mm, respectively.

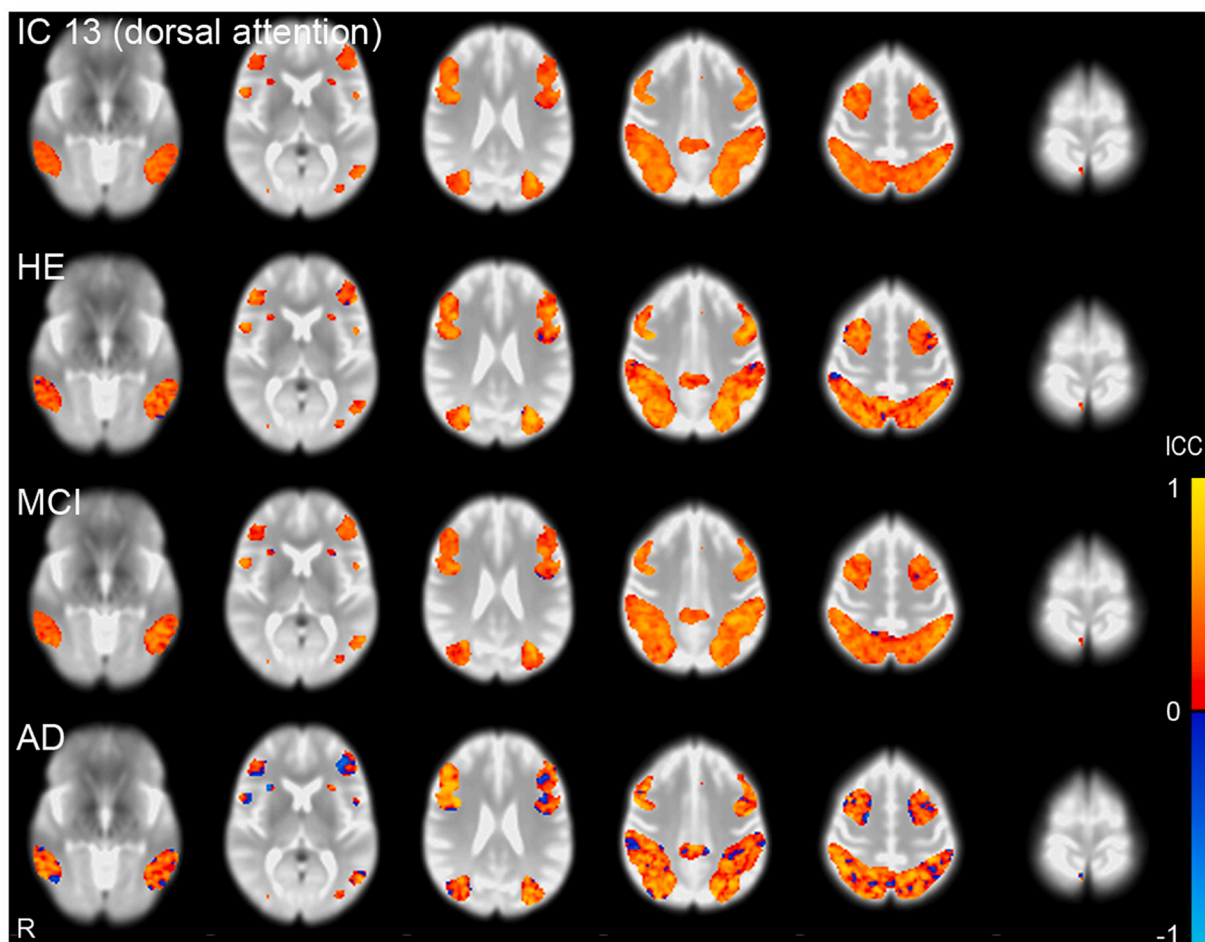


Fig. 4. (continued).

4. Discussion

In the present study, we examined the long-term (1-year) test-retest reliability of RSNs in healthy elderly subjects, patients with MCI, and patients with AD using temporal concatenation group ICA and dual regression. The test-retest reliability was generally lower in patients with MCI than in healthy elderly subjects, and was lower in patients with AD than in patients with MCI. The results indicate that the differences in test-retest reliability of RSNs among these three groups were mainly due to the differences in the test-retest reliability of RSN amplitudes rather than those of RSN shapes.

The results of the present study suggest that test-retest stability of RSNs declines with progression to MCI and to AD, even in regions relatively unaffected until late in the disease. The test-retest variability of RSN shapes was almost the same among healthy elderly subjects, patients with MCI, and patients with AD, whereas the test-retest stability of RSN amplitudes generally declined with progression to MCI and to AD. This indicates that the test-retest variability of functional connectivity between regions of each RSN is relatively not different among healthy elderly, MCI, and AD, and that disease progression affects the test-retest variability of overall functional connectivity of the RSN.

4.1. Test-Retest Reliability of RSNs in MCI and AD

Although previous studies have evaluated the test-retest reliability

of rs-fMRI, mainly in young to middle-aged healthy subjects [21–25], few studies have focused on healthy elderly subjects [26–30], patients with MCI [31,32], or patients with AD [33].

Blautzik et al. [32] investigated the long-term (approximately 13–16 months) test-retest reliability of RSNs in 12 healthy control subjects (mean age, 67.8 ± 7.3 years [range, 59–83 years]) and 13 patients with amnestic MCI (mean age, 72.8 ± 7.3 years [range, 60–88 years]) using 3.0 T MRI, with temporal concatenation group ICA and dual regression. The test-retest reliability of each RSN was determined by calculating the voxel-wise ICCs and was expressed as the most frequent ICC ("modal ICC"). The overall test-retest reliability of RSNs was higher in the healthy control group (mean "modal ICC", 0.52 [range, 0.33–0.65]) than in the MCI group (mean "modal ICC", 0.38 [range, 0.23–0.58]). The RSNs were most reliable in the healthy control group and were associated with sensory and motor as well as higher-order cognitive and the default mode function. The authors concluded that stable RSNs may represent healthy aging, while decreased RSN reliability may indicate progressive neurofunctional alterations before the manifestation of clinical symptoms.

Conwell et al. [31] investigated the short-term (approximately 2 weeks) test-retest reliability of three memory-related RSNs (default mode, salience, and executive control networks) in 15 young subjects (mean age, 24.4 ± 2.8 years), 15 healthy senior subjects (mean age, 67.3 ± 8.1 years), and 15 patients with MCI positive for biomarkers suggestive of prodromal AD (mean age, 71.1 ± 6.0 years) using 3.0 T

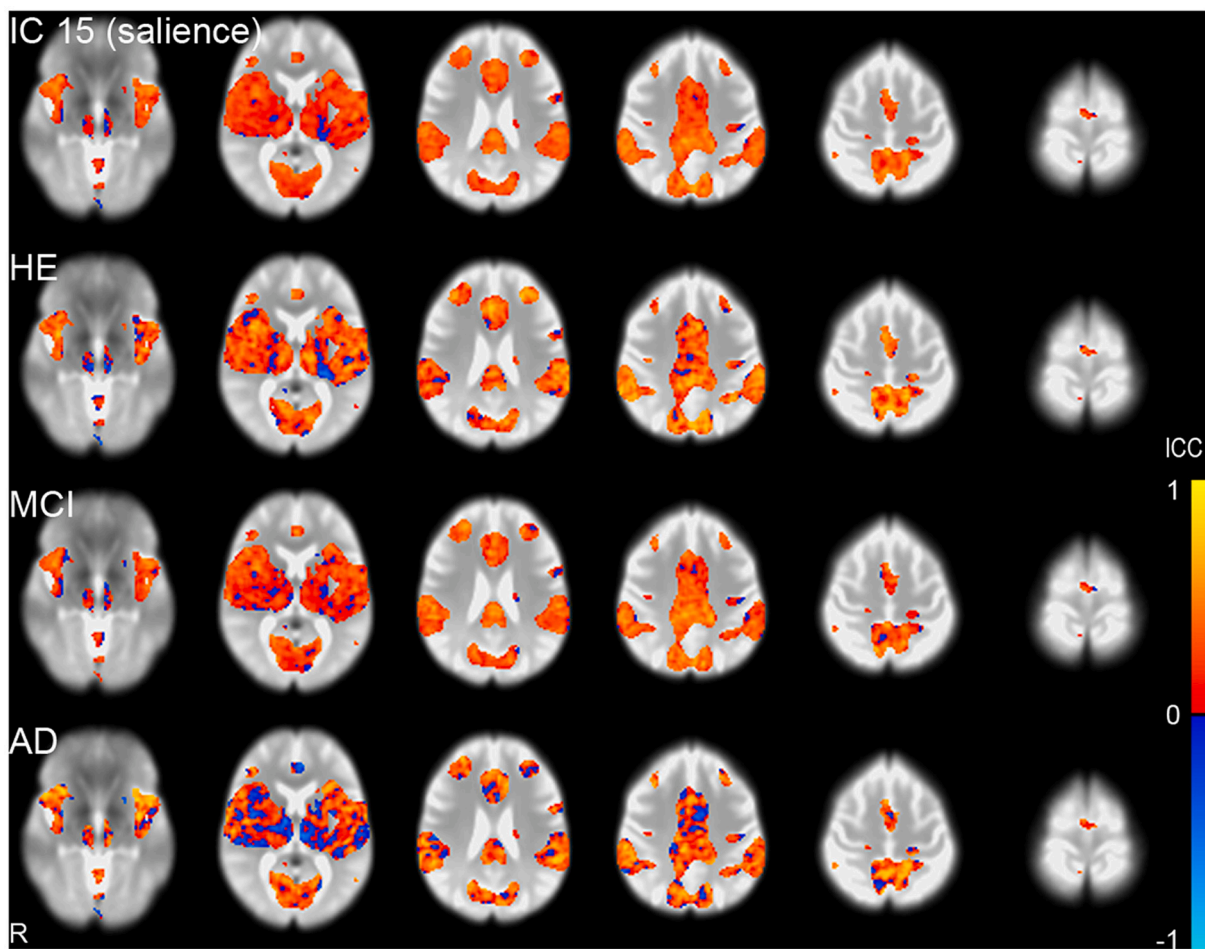


Fig. 4. (continued).

MRI, with temporal concatenation group ICA and back reconstruction (GICA3). The test-retest reliability was evaluated by voxel-wise ICCs, in which the voxel-wise time series were used to calculate ICCs within the RSNs. The test-retest reliability of RSNs was generally higher in the young subjects (mean ICC, 0.40–0.53) than in the healthy senior subjects (mean ICC, 0.35–0.46) and patients with MCI (mean ICC, 0.34–0.42).

In the present study, we examined the 1-year test-retest reliability of RSNs in 31 healthy elderly subjects, 63 patients with MCI, and 17 patients with AD using 3.0 T ADNI 2 data, with temporal concatenation group ICA and dual regression. Overall, the test-retest reliability was lower in patients with AD and higher in healthy elderly subjects. The test-retest reliability of RSNs generally declined with progression to MCI and to AD, and the differences in the test-retest reliability of RSNs were mainly due to the RSN amplitudes rather than the RSN shapes.

4.2. Factors Affecting the Test–Retest Reliability of RSNs

Neural and non-neural factors may contribute to the intrasubject variability in resting-state functional connectivity. Functional connectivity is not static, and the connection strengths vary during a single imaging session at rest and between sessions, and between different cognitive tasks [47]. Non-neural factors that may affect intrasubject variability of resting-state functional connectivity include scan conditions, head motion, physiological noise, and data analysis/standardization strategies [48]. Non-neural factors that contribute to the BOLD time series include thermal noise inherent to the electrical circuits used for MR signal reception, instrument drift, artifact signals due to

hardware instabilities, and signal changes due to head motion, as well as various non-neural physiological factors like cardiac and respiratory noise, changes in the arterial CO₂ concentration associated with varying respiration rates, vasomotion, and changes in blood pressure and cerebral autoregulation [49,50].

Because the present study included elderly subjects and patients with MCI or AD, head motion could be a non-neural factor most affecting the test–retest reliability of RSNs; however, head motion was generally similar among the three groups of subjects. Thus, the test–retest instability in patients with MCI and AD may reflect progressive neurofunctional alterations related to AD pathology.

4.3. Limitations

The present study had several limitations. First, this study used rsfMRI data with the interval of 1 year to evaluate the long-term test–retest reliability of RSNs. The changes in non-neuronal factors other than head motion may affect intrasubject variability of resting-state functional connectivity. Second, test–retest variability of RSNs may differ between MCI patients with and without conversion to dementia. It is an interesting topic, but somewhat beyond the scope of this study. Finally, this study did not evaluate the effect of brain atrophy on the long-term test–retest reliability of RSNs. It is well known that patients with Alzheimer's disease have accelerated brain atrophy. Brain atrophy occurs earliest in the medial temporal lobe (hippocampus and entorhinal cortex) and subsequently extends along a temporal–parietal–frontal trajectory. Sensorimotor and visual cortices are unaffected

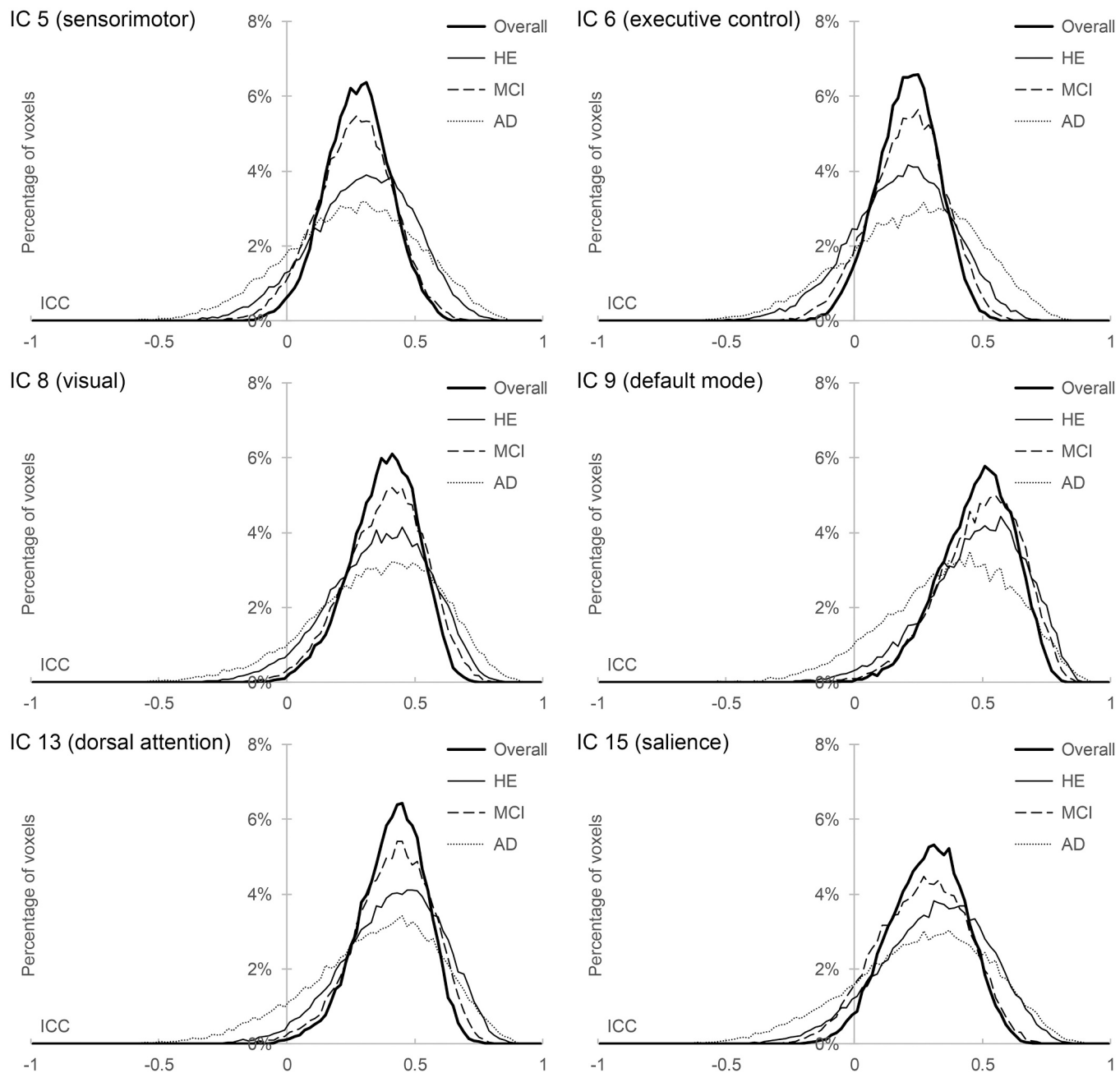


Fig. 5. Histograms (frequency polygons) of voxel-wise intraclass correlation coefficient (ICC) maps of subject-specific spatial maps without variance normalization of the subject-specific time courses during dual regression, representing resting-state network shapes. IC, independent component; HE, healthy elderly; MCI, mild cognitive impairment; AD, Alzheimer's disease.

Table 7

Peaks in the histograms of intraclass correlation coefficient maps of subject-specific spatial maps without variance normalization of the subject-specific time courses during dual regression, representing resting-state network shapes.

	Overall	HE	MCI	AD
IC 5 (sensorimotor)	0.30–0.32	0.30–0.32	0.26–0.28	0.28–0.30
IC 6 (executive control)	0.24–0.26	0.20–0.22	0.24–0.26	0.26–0.28
IC 8 (visual)	0.40–0.42	0.44–0.46	0.40–0.42	0.40–0.42
IC 9 (default mode)	0.50–0.52	0.56–0.58	0.54–0.56	0.44–0.46
IC 13 (dorsal attention)	0.44–0.46	0.48–0.50	0.44–0.46	0.44–0.46
IC 15 (salience)	0.30–0.32	0.30–0.32	0.26–0.28	0.36–0.38

IC, independent component; HE, healthy elderly; MCI, mild cognitive impairment; AD, Alzheimer's disease.

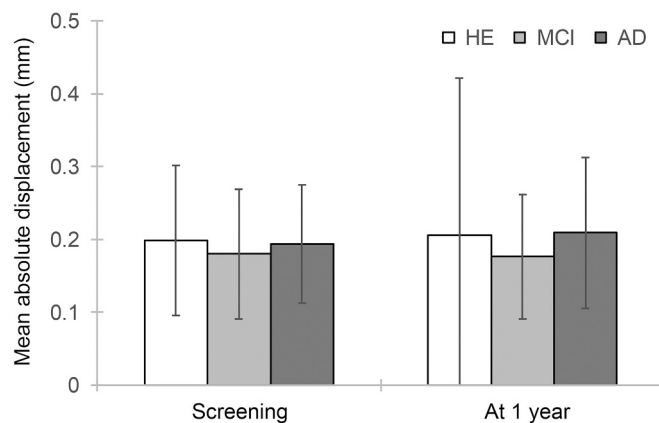


Fig. 6. Mean absolute and relative displacements (mean \pm standard deviation), representing head motion during scanning. HE, healthy elderly; MCI, mild cognitive impairment; AD, Alzheimer's disease.

until late in the disease. Accelerated brain atrophy may have the potential to affect the test-retest reliability of RSNs; however, this study showed a decline in the test-retest stability of RSNs with progression to MCI and to AD, even in regions spared until late in the disease.

5. Conclusions

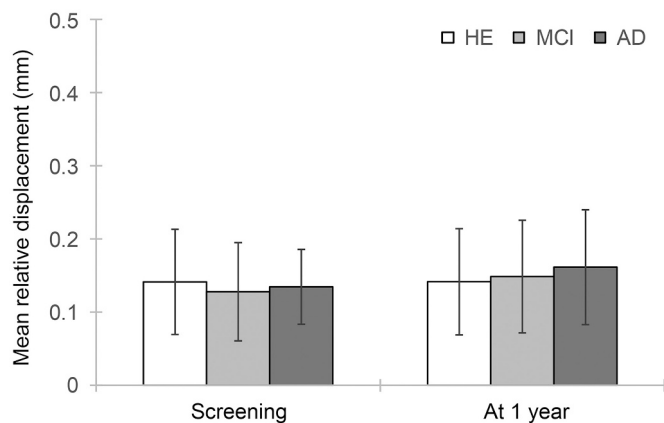
In this study, we examined the long-term (1-year) test-retest reliability of RSNs in healthy elderly subjects, patients with MCI, and patients with AD. Our results indicate that the test-retest stability of RSNs generally declines with progression to MCI and to AD, and the differences in test-retest reliability of RSNs are likely due to the RSN amplitudes rather than the RSN shapes. The test-retest instability in MCI and AD may reflect progressive neurofunctional alterations due to the pathology of AD.

Declarations of interest

None.

Acknowledgements

Data collection and sharing for this project was funded by the Alzheimer's Disease Neuroimaging Initiative (ADNI) (National Institutes of Health Grant U01 AG024904) and DOD ADNI (Department of Defense award number W81XWH-12-2-0012). ADNI is funded by the National Institute on Aging, the National Institute of Biomedical Imaging and Bioengineering, and through generous contributions from the following: AbbVie, Alzheimer's Association; Alzheimer's Drug Discovery Foundation; Araclon Biotech; BioClinica, Inc.; Biogen; Bristol-Myers Squibb Company; CereSpir, Inc.; Cogstate; Eisai Inc.; Elan Pharmaceuticals, Inc.; Eli Lilly and Company; EuroImmun; F. Hoffmann-La Roche Ltd. and its affiliated company Genentech, Inc.; Fujirebio; GE Healthcare; IXICO Ltd.; Janssen Alzheimer Immunotherapy Research & Development, LLC.; Johnson & Johnson Pharmaceutical Research & Development LLC.; Lumosity; Lundbeck; Merck & Co., Inc.; Meso Scale Diagnostics, LLC.; NeuroRx Research; Neurotrack Technologies; Novartis Pharmaceuticals Corporation; Pfizer Inc.; Piramal Imaging; Servier; Takeda Pharmaceutical Company; and Transition Therapeutics. The Canadian Institutes of Health Research is providing funds to support ADNI clinical sites in Canada. Private sector contributions are facilitated by the Foundation for the National Institutes of Health (<https://www.fnih.org>). The grantee organization is the Northern California Institute for Research and Education, and the study is coordinated by the Alzheimer's Therapeutic Research Institute at the University of Southern California. ADNI data are disseminated by the Laboratory for Neuro Imaging at the



University of Southern California.

References

- [1] Biswal B, Yetkin FZ, Haughton VM, Hyde JS. Functional connectivity in the motor cortex of resting human brain using echo-planar MRI. *Magn Reson Med* 1995;34(4):537–41.
- [2] Pietzsch M, King AE, Ward DD, Vickers JC. The influence of genetic factors and cognitive reserve on structural and functional resting-state brain networks in aging and Alzheimer's disease. *Front Aging Neurosci* 2019;11:30.
- [3] Jack Jr CR, Knopman DS, Jagust WJ, Petersen RC, Weiner MW, Aisen PS, et al. Tracking pathophysiological processes in Alzheimer's disease: an updated hypothetical model of dynamic biomarkers. *Lancet Neurol* 2013;12(2):207–16.
- [4] Barkhof F, Haller S, Rombouts SA. Resting-state functional MR imaging: a new window to the brain. *Radiology* 2014;272(1):29–49.
- [5] Forouzannezhad P, Abbaspour A, Fang C, Cabrerizo M, Loewenstein D, Duara R, et al. A survey on applications and analysis methods of functional magnetic resonance imaging for Alzheimer's disease. *J Neurosci Methods* 2019;317:121–40.
- [6] Hohenfeld C, Werner CJ, Reetz K. Resting-state connectivity in neurodegenerative disorders: is there potential for an imaging biomarker? *NeuroImage Clin* 2018;18:849–70.
- [7] Jovicich J, Czanner S, Han X, Salat D, van der Kouwe A, Quinn B, et al. MRI-derived measurements of human subcortical, ventricular and intracranial brain volumes: reliability effects of scan sessions, acquisition sequences, data analyses, scanner upgrade, scanner vendors and field strengths. *Neuroimage* 2009;46(1):177–92.
- [8] Takao H, Hayashi N, Ohtomo K. Effect of scanner in longitudinal studies of brain volume changes. *J Magn Reson Imaging* 2011;34(2):438–44.
- [9] Takao H, Hayashi N, Ohtomo K. Effects of the use of multiple scanners and of scanner upgrade in longitudinal voxel-based morphometry studies. *J Magn Reson Imaging* 2013;38(5):1283–91.
- [10] Dickerson BC, Fenstermacher E, Salat DH, Wolk DA, Maguire RP, Desikan R, et al. Detection of cortical thickness correlates of cognitive performance: reliability across MRI scan sessions, scanners, and field strengths. *Neuroimage* 2008;39(1):10–8.
- [11] Takao H, Hayashi N, Ohtomo K. Effects of study design in multi-scanner voxel-based morphometry studies. *Neuroimage* 2014;84:133–40.
- [12] Takao H, Hayashi N, Ohtomo K. Brain morphology is individual-specific information. *Magn Reson Imaging* 2015;33(6):816–21.
- [13] Shuter B, Yeh IB, Graham S, Au C, Wang SC. Reproducibility of brain tissue volumes in longitudinal studies: effects of changes in signal-to-noise ratio and scanner software. *Neuroimage* 2008;41(2):371–9.
- [14] Takao H, Amemiya S, Abe O. Reliability of changes in brain volume determined by longitudinal voxel-based morphometry. *J Magn Reson Imaging* 2021. <https://doi.org/10.1002/jmri.27568>.
- [15] Takao H, Amemiya S, Abe O. Reproducibility of brain volume changes in longitudinal voxel-based morphometry between non-accelerated and accelerated magnetic resonance imaging. *J Alzheimers Dis* 2021. <https://doi.org/10.3233/JAD-210596>. In press.
- [16] Danielian LE, Iwata NK, Thomasson DM, Floeter MK. Reliability of fiber tracking measurements in diffusion tensor imaging for longitudinal study. *Neuroimage* 2010;49(2):1572–80.
- [17] Takao H, Hayashi N, Kabasawa H, Ohtomo K. Effect of scanner in longitudinal diffusion tensor imaging studies. *Hum Brain Mapp* 2012;33(2):466–77.
- [18] Takao H, Hayashi N, Ohtomo K. Effect of scanner in asymmetry studies using diffusion tensor imaging. *Neuroimage* 2011;54(2):1053–62.
- [19] Lemkadem A, Daducci A, Vulliemoz S, O'Brien K, Lazeyras F, Hauf M, et al. A multi-center study: intra-scan and inter-scan variability of diffusion spectrum imaging. *Neuroimage* 2012;62(1):87–94.

- [20] Takao H, Hayashi N, Ohtomo K. Brain diffusivity pattern is individual-specific information. *Neuroscience* 2015;301:395–402.
- [21] Zhang C, Baum SA, Adduru VR, Biswal BB, Michael AM. Test-retest reliability of dynamic functional connectivity in resting state fMRI. *Neuroimage* 2018;183:907–18.
- [22] Noble S, Spann MN, Tokoglu F, Shen X, Constable RT, Scheinost D. Influences on the test-retest reliability of functional connectivity MRI and its relationship with behavioral utility. *Cereb Cortex* 2017;27(11):5415–29.
- [23] Fiecas M, Ombao H, van Lunen D, Baumgartner R, Coimbra A, Feng D. Quantifying temporal correlations: a test-retest evaluation of functional connectivity in resting-state fMRI. *Neuroimage* 2013;65:231–41.
- [24] Seibert TM, Majid DS, Aron AR, Corey-Bloom J, Brewer JB. Stability of resting fMRI interregional correlations analyzed in subject-native space: a one-year longitudinal study in healthy adults and premanifest Huntington's disease. *Neuroimage* 2012;59(3):2452–63.
- [25] Zuo XN, Kelly C, Adelstein JS, Klein DF, Castellanos FX, Milham MP. Reliable intrinsic connectivity networks: test-retest evaluation using ICA and dual regression approach. *Neuroimage* 2010;49(3):2163–77.
- [26] Marchitelli R, Minati L, Marizzoni M, Bosch B, Bartres-Faz D, Muller BW, et al. Test-retest reliability of the default mode network in a multi-centric fMRI study of healthy elderly: effects of data-driven physiological noise correction techniques. *Hum Brain Mapp* 2016;37(6):2114–32.
- [27] Jovicich J, Minati L, Marizzoni M, Marchitelli R, Sala-Llonch R, Bartres-Faz D, et al. Longitudinal reproducibility of default-mode network connectivity in healthy elderly participants: a multicentric resting-state fMRI study. *Neuroimage* 2016;124 (Pt A):442–54.
- [28] Guo CC, Kurth F, Zhou J, Mayer EA, Eickhoff SB, Kramer JH, et al. One-year test-retest reliability of intrinsic connectivity network fMRI in older adults. *Neuroimage* 2012;61(4):1471–83.
- [29] Ousdal OT, Kaufmann T, Kolskar K, Vik A, Wehling E, Lundervold AJ, et al. Longitudinal stability of the brain functional connectome is associated with episodic memory performance in aging. *Hum Brain Mapp* 2020;41(3):697–709.
- [30] Song J, Desphande AS, Meier TB, Tudorascu DL, Verguts S, Nair VA, et al. Age-related differences in test-retest reliability in resting-state brain functional connectivity. *PLoS One* 2012;7(12):e49847.
- [31] Conwell K, von Reutern B, Richter N, Kukolja J, Fink GR, Onur OA. Test-retest variability of resting-state networks in healthy aging and prodromal Alzheimer's disease. *NeuroImage Clin* 2018;19:948–62.
- [32] Blautzik J, Keeser D, Berman A, Paolini M, Kirsch V, Mueller S, et al. Long-term test-retest reliability of resting-state networks in healthy elderly subjects and with amnestic mild cognitive impairment patients. *J Alzheimers Dis* 2013;34(3):741–54.
- [33] Postema MC, De Marco M, Colato E, Venneri A. A study of within-subject reliability of the brain's default-mode network. *Magma* 2019;32(3):391–405.
- [34] Nickerson LD, Smith SM, Ongur D, Beckmann CF. Using dual regression to investigate network shape and amplitude in functional connectivity analyses. *Front Neurosci* 2017;11:115.
- [35] Sled JG, Zijdenbos AP, Evans AC. A nonparametric method for automatic correction of intensity nonuniformity in MRI data. *IEEE Trans Med Imaging* 1998;17(1):87–97.
- [36] Takao H, Abe O, Hayashi N, Kabasawa H, Ohtomo K. Effects of gradient non-linearity correction and intensity non-uniformity correction in longitudinal studies using structural image evaluation using normalization of atrophy (SIENA). *J Magn Reson Imaging* 2010;32(2):489–92.
- [37] Takao H, Abe O, Ohtomo K. Computational analysis of cerebral cortex. *Neuroradiology* 2010;52(8):691–8.
- [38] Smith SM, Jenkinson M, Woolrich MW, Beckmann CF, Behrens TE, Johansen-Berg H, et al. Advances in functional and structural MR image analysis and implementation as FSL. *Neuroimage* 2004;23(Suppl. 1):S208–19.
- [39] Jenkinson M, Bannister P, Brady M, Smith S. Improved optimization for the robust and accurate linear registration and motion correction of brain images. *Neuroimage* 2002;17(2):825–41.
- [40] Smith SM. Fast robust automated brain extraction. *Hum Brain Mapp* 2002;17(3):143–55.
- [41] Greve DN, Fischl B. Accurate and robust brain image alignment using boundary-based registration. *Neuroimage* 2009;48(1):63–72.
- [42] Beckmann CF, Smith SM. Probabilistic independent component analysis for functional magnetic resonance imaging. *IEEE Trans Med Imaging* 2004;23(2):137–52.
- [43] Smith SM, Fox PT, Miller KL, Glahn DC, Fox PM, Mackay CE, et al. Correspondence of the brain's functional architecture during activation and rest. *Proc Natl Acad Sci U S A* 2009;106(31):13040–5.
- [44] Hyvärinen A. Fast and robust fixed-point algorithms for independent component analysis. *IEEE Trans Neural Netw* 1999;10(3):626–34.
- [45] Koo TK, Li MY. A guideline of selecting and reporting intraclass correlation coefficients for reliability research. *J Chiropr Med* 2016;15(2):155–63.
- [46] McGraw KO, Wong SP. Forming inferences about some intraclass correlation coefficients. *Psychol Methods* 1996;1(1):30–46.
- [47] Finn ES, Scheinost D, Finn DM, Shen X, Papademetris X, Constable RT. Can brain state be manipulated to emphasize individual differences in functional connectivity? *Neuroimage* 2017;160:140–51.
- [48] Zuo XN, Xing XX. Test-retest reliabilities of resting-state fMRI measurements in human brain functional connectomics: a systems neuroscience perspective. *Neurosci Biobehav Rev* 2014;45:100–18.
- [49] Murphy K, Birn RM, Bandettini PA. Resting-state fMRI confounds and cleanup. *Neuroimage* 2013;80:349–59.
- [50] Caballero-Gaudes C, Reynolds RC. Methods for cleaning the BOLD fMRI signal. *Neuroimage* 2017;154:128–49.